Supporting Information

Unraveling the Origin of the Long Fluorescence Decay Component of Cesium Lead Halide Perovskite Nanocrystals

Michael A. Becker,[1,2] Caterina Bernasconi,[3,4] Maryna I. Bodnarchuk,[3,4] Gabriele Rainò,[3,4] Maksym V. Kovalenko[3,4], David J. Norris[2], Rainer F. Mahrt[1] and Thilo Stöferle[1]

[1] IBM Research Europe – Zurich, Säumerstrasse 4, 8803 Rüschlikon, Switzerland.

[2] Optical Materials Engineering Laboratory, Department of Mechanical and Process Engineering, ETH Zurich, 8092 Zurich, Switzerland.

[3] Laboratory for Thin Films and Photovoltaics, Empa, Swiss Federal Laboratories for Materials Science and Technology, 8600 Dübendorf, Switzerland.

[4] Institute of Inorganic Chemistry, Department of Chemistry and Applied Biosciences, ETH Zurich, 8093 Zurich, Switzerland.

S1. Blinking-Free Emission of $CsPbBr_2Cl$ Nanocrystals

Compared with the relatively small $CsPbBr_3$ nanocrystals studied in the main text, $CsPbBr_2Cl$ and large $CsPbBr_3$ nanocrystals typically show a different intermittency behavior.[1] Figure S1a displays an intensity–time curve of a single $CsPbBr_2Cl$ quantum dot, binned with a time resolution of 10 ms, recorded at a temperature of 5 K. The quantum dot was excited by a pulsed laser with a repetition rate of 40 MHz at a photon energy of 3.06 eV and an excitation fluence of 0.2 μJ cm^{-2}, essentially the same conditions as for the $CsPbBr_3$ nanocrystals. Within the

measurement time of 500 s, we do not observe any blinking events or abrupt switches of intensity, evidencing that the quantum dot seems to be in a constant “on”-state. The intensity-distribution histogram shown in Figure S1b, follows a slightly broadened Poissonian distribution (red line). The origin of the broadening is most likely due to spatial drift of the sample during the acquisition time, since the overall intensity increases slightly with time in this measurement, presumably drifting closer to the center of the excitation beam. The distribution is fitted best with a Gaussian function (green line). Although we clearly observe blinking-free emission from a single quantum dot, we see that the spectrum of a single quantum dot (Figure S1c) acquired with 1 s exposure time is composed of an exciton emission at 2.603 eV exhibiting two emission peaks with a clear fine structure splitting of 1 meV and a trion emission peak red-shifted by 15 meV compared to the exciton emission center energy. This is counterintuitive, since blinking is mainly attributed to Auger quenching of a biexciton or trion state, and therefore, fluorescence intermittency should be apparent when trion emission is observed. The simultaneous and constant observation of exciton and trion emission (see also ref. 1-3) on a second-time scale implies that trapping and detrapping, responsible for blinking, occurs mainly on a sub-second time scale. Figure S1d displays the spectrally integrated emission intensity as a function of almost two orders of magnitude variation in excitation density. The emitted intensity follows a power-law dependence with an exponent of 0.94±0.01, indicating that nonradiative recombination mechanisms like Auger recombination are almost absent in this excitation-power range. Hence, the reason for not observing blinking in Figure S1a might be either that blinking occurs on time scales much faster than 10 ms or that we do not observe blinking events because trion emission has also unity quantum yield. Hence, to observe emission of excitons and trions from the same quantum dot without any evidences of Auger-like processes, trapping and detrapping processes must occur. These processes probably occur with a very high rate, such that we do not observe a switching between exciton and trion

emission on time scales comparable with the typical acquisition times in our measurement setup.

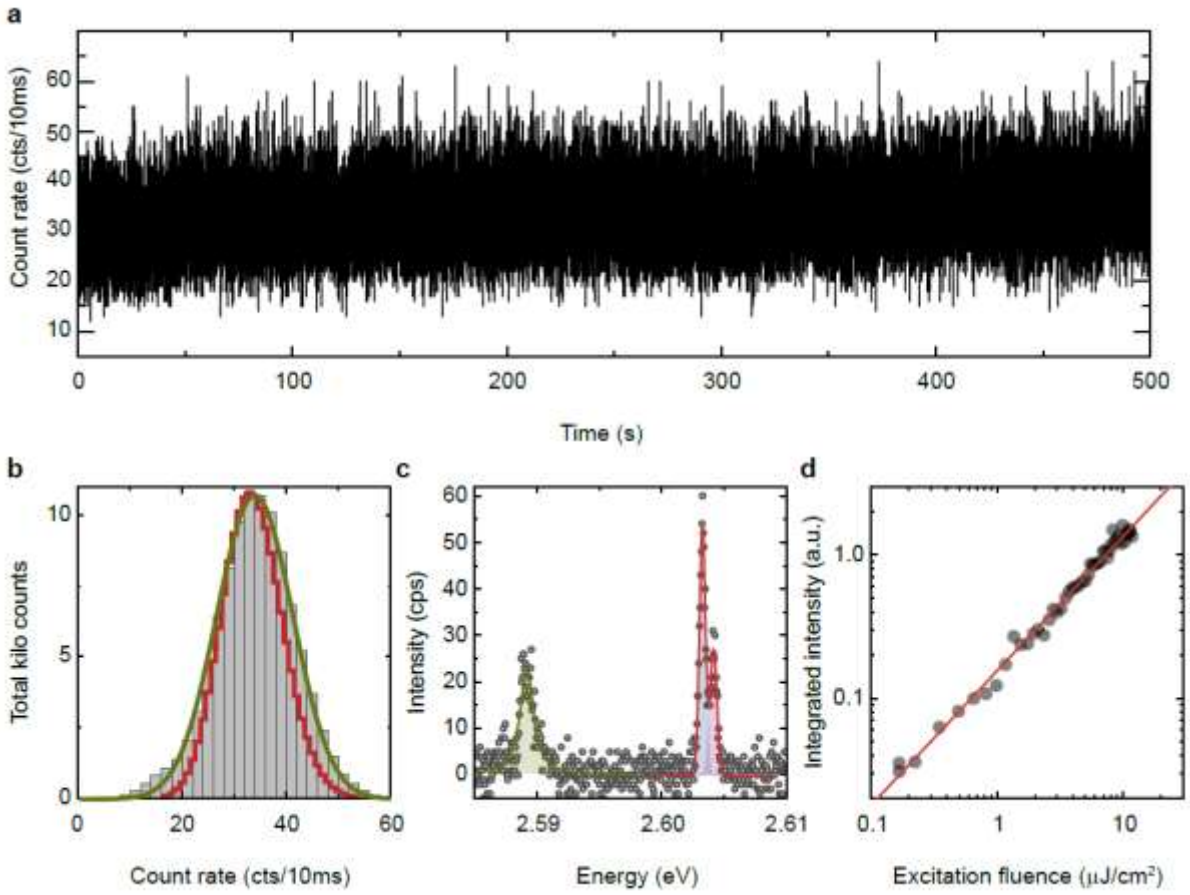

Figure S1. Blinking-free emission of $CsPbBr_2Cl$ nanocrystals. (a) Intensity–time trace of a single $CsPbBr_2Cl$ nanocrystal, binned with a time resolution of 10 ms, recorded at 5 K. (b) Intensity-distribution histogram of the intensity–time curve in (a) fitted with a Poissonian (red) and Gaussian (green) intensity distribution. (c) Photoluminescence spectrum of a single $CsPbBr_2Cl$ quantum dot exhibiting an exciton emission at 2.603 eV with a fine structure splitting of 1 meV and a trion emission peak that is red-shifted by 15 meV with Lorentzian curve function fits in red and green, respectively. (d) Spectrally integrated emission intensity as a function of the excitation density of the blue laser. The integrated intensity follows a power-law dependence with an exponent of 0.94±0.01.

S2. Nanocrystal Size Distribution

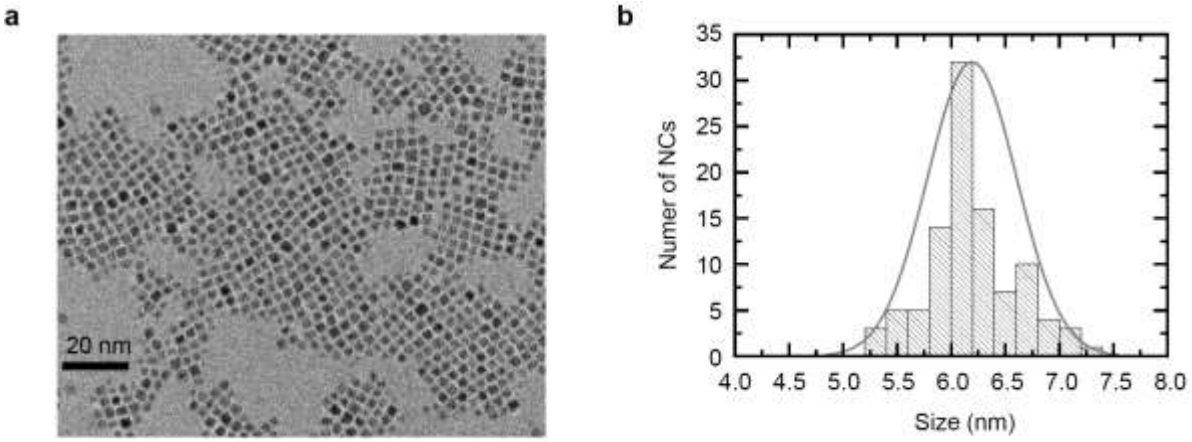

Figure S2. TEM image and size statistics obtained from the same batch of nanocrystals. (a) TEM image of $CsPbBr_3$ nanocrystals synthesized in the same way as the measured sample. (b) Nanocrystal size distribution with an average size of 6.2±0.4 nm.

S3. Flickering of $CsPbBr_3$ Nanocrystals

In many intensity–time traces we observe strong photoluminescence-intensity fluctuations, referred to as flickering. In Figure S3a we exemplarily show an intensity–time trace of a single $CsPbBr_3$ quantum dot with a size of 12 nm. In these time traces, it is not possible to distinguish between two (or more) intensity levels, but quasi-continuous intensity fluctuations are observed.[4,5] One reason for the characteristic flickering behavior is a fast (sub-millisecond) switching between the exciton and trion state, leading to contributions from both states in every time bin. This can be also observed in the intensity-dependent photoluminescence decay traces of bins in the range 0 – 50 counts per 10 ms (red) and 75 – 150 counts per 10 ms (gray), shown in Figure S3b. The two decay traces obtain a high degree of similarity since the exponential

(τ_{gray} = 320 ps and τ_{red} = 240 ps) and power-law decay components (α_{gray} = -0.6 and α_{red} = -0.7) are rather similar, but show that for the low-intensity levels the relative contribution of the trion state is higher compared to the high-intensity levels. Furthermore, we observe that for the decay trace of the low-intensity levels, the relative contribution of the delayed fluorescence is higher.

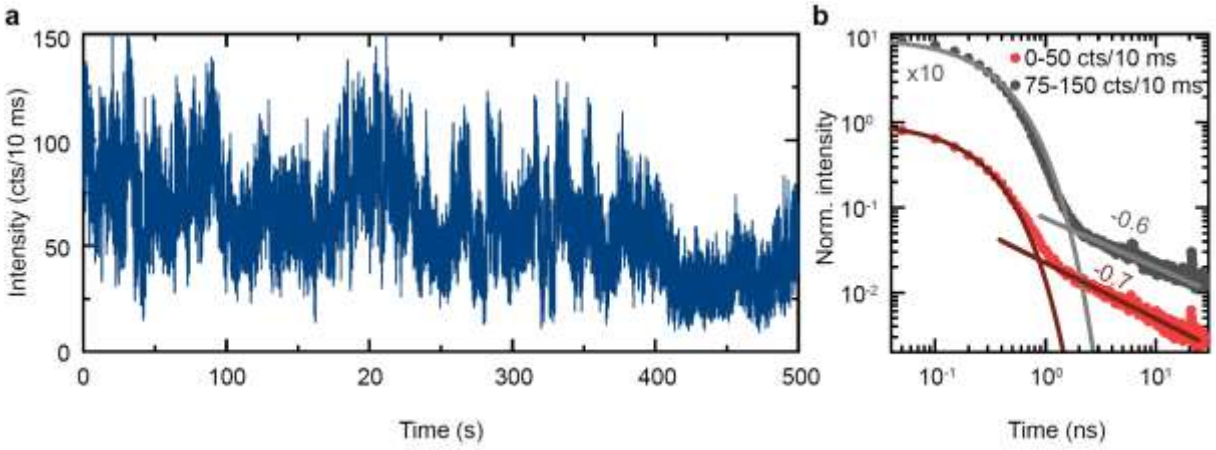

Figure S3. Blinking and flickering in $CsPbBr_3$ quantum dots. (a) Intensity–time trace of a single $CsPbBr_3$ quantum dot with a size of 12 nm. (b) Normalized photoluminescence decay of the high- and low-intensity bins in gray and red, respectively.

S4. Additional Data on Single $CsPbBr_3$ Nanocrystals

In Figure S4, we display additional TTTR3 data of several single $CsPbBr_3$ nanocrystals. In the left panels, the normalized intensity–time traces with 100-ms bins are displayed. All intensity–time traces show blinking/flickering on millisecond-to-second time scales. The low-intensity level shows a strong quantum dot-to-quantum dot variation. From the intensity–time trace, we extracted the normalized high- (gray) and low-intensity (red) photoluminescence decays in the right panels. The high and low intensities are color-coded with the gray and red area in the intensity–time trace, respectively. The exponents of the long decay components vary from

quantum dot to quantum dot but are all within the same range. The exponent of the low-intensity photoluminescence decay is always smaller compared to the high-intensity photoluminescence decay, as also seen with the quantum dot data discussed in more detail in the main text.

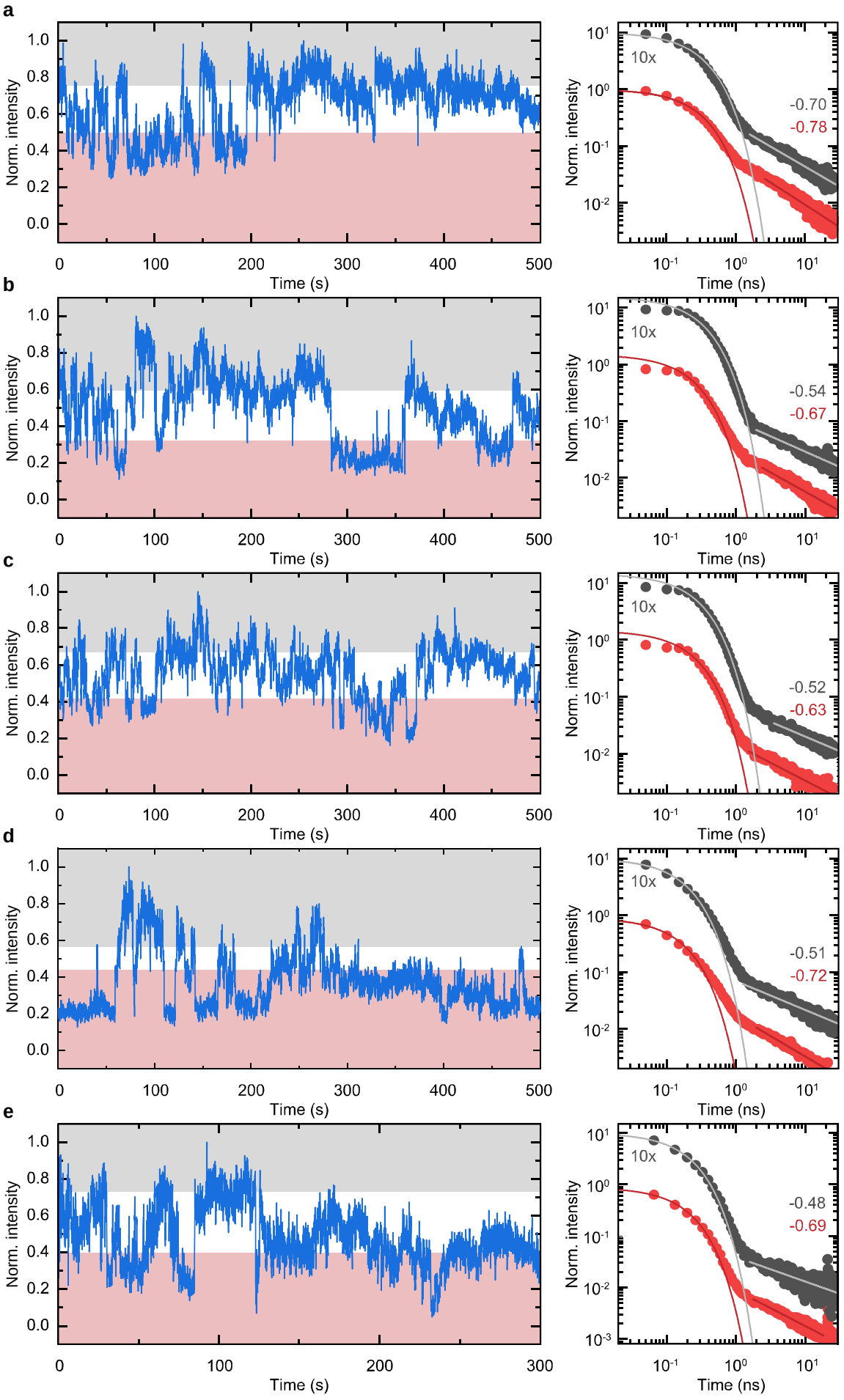
a
b
c
d
e
Norm. intensity
Time (s)
Time (ns)
10x
-0.70
-0.78
-0.54
-0.67
-0.52
-0.63
-0.51
-0.72
-0.48
-0.69

Figure S4. TTTR3 data of 5 single $CsPbBr_3$ nanocrystals. Left panels: Intensity–time traces for different quantum dots with a 100-ms bin. Right panels: Corresponding photoluminescence decay traces for the high- and low-intensity bins marked in the left panel with the gray and red area, respectively.

S5. Fluorescence Background

To make sure that the presented measurements are not affected by background luminescence from the substrate, we recorded the background luminescence on a sample prepared in the same way in an area without quantum dots in the polymer film with an excitation density of 0.4 μJ cm^{-2} at a repetition rate of 20 MHz and through the same narrow bandpass filters. In Figure S5a, we display the intensity–time trace of the background luminescence with a bin size of 10 ms. The average intensity is close to 1 count per 10 ms, indicated by the horizontal red bar in this Figure and in the main manuscript in Figures 3a and b by horizontal gray bars. This average background luminescence is significantly below the signal of the quantum dot, even when it is in a low-intensity state. To visualize this in more detail, Figure S5b shows the photoluminescence decay of the low-intensity state averaged over 10 s (during the longest low-intensity period in Figure 3a) in units of counts per second (cts/s), as well as the time-resolved background signal. The background signal decays on a nanosecond time scale with a time constant different from the measured decay constants of the exciton and trion decay, as well as the long decay components of the high- and low-intensity states. Due to the decay, we assume that the fluorescence is mainly background fluorescence from the substrate, the polymer matrix or residuals from the solvent. However, from this plot it is evident that at all times after the excitation pulse, the signal – even in the low-intensity state – is almost an order of magnitude

higher compared to the background signal, and hence, we can safely exclude any influence of the background fluorescence in the measurement.

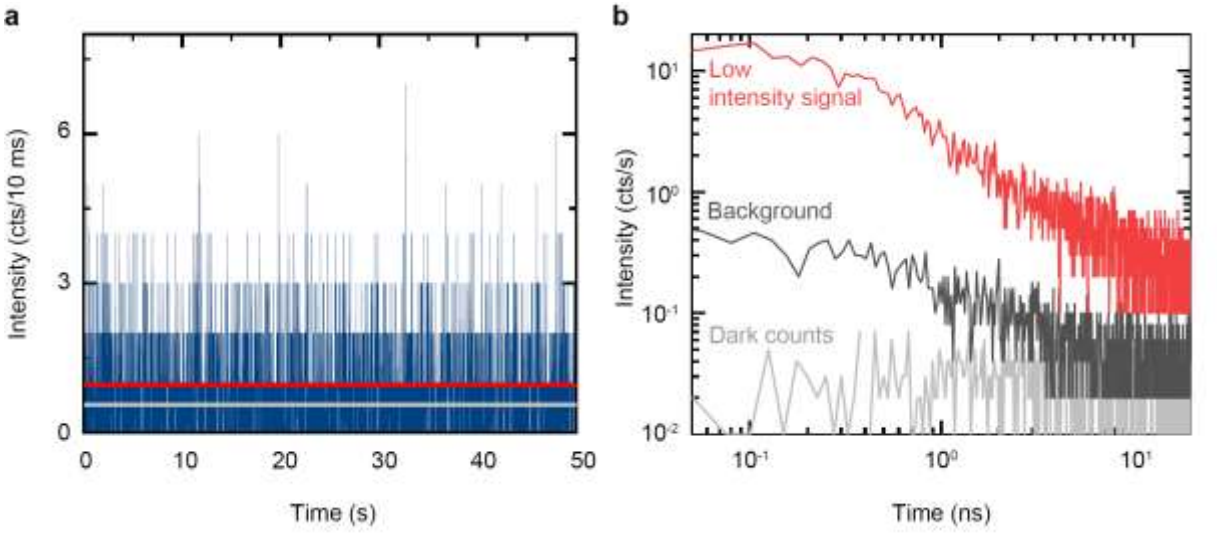

Figure S5. Background luminescence. (a) Intensity–time trace of a sample without quantum dots recorded over 50 s under the identical excitation conditions as in the measurements from Figure 3. The average intensity is shown as the red horizontal line. The average measured dark counts (acquired with no excitation beam) are indicated as the gray horizontal line. (b) Time-dependent photoluminescence decay in counts per second of the dark counts, of the background and of a low-intensity period averaged over 10 s from Figure 3a.

S6. Microscopic Blinking Model

To explain the origin of the delayed fluorescence of the low-intensity trion peak, one has to include additional mechanisms to existing models. Our model presented here is based on the fundamental charging model proposed by Efros and Rosen[6] and extended by Ye *et al.*, considering multi-excitons.[7] In Figure 5 we display the basic model that we use to explain our

observations. One of the main processes investigated in colloidal quantum dots is the radiative emission from a single exciton state (X). Therefore, the ground state (G) is excited by a laser with the repetition rate Γ_{Rep}, and an exciton is generated with a probability n_X. From the ground state, it is in principle also possible to directly generate a biexciton state (XX) with a probability n_{XX} or multi-exciton states (n_{NX}) that are not included in this model. The possibility to directly generate a biexciton state is negligible. However, we assume it to be roughly 5% of the exciton generation probability. The single exciton state can radiatively recombine with a rate $\Gamma_X = 1/\tau_X = 2.5 \cdot 10^{-3}$ ps^{-1}, corresponding to the decay time τ that we measure for perovskite nanocrystals. However, in the excited state X, one of the charge carriers can get trapped with a trapping rate $\Gamma_{X,trap}$ in a so-called charge-separated state,[8] leaving behind one delocalized charge in the quantum dot. The trapped charge can detrap, and the single exciton state can be recovered, giving rise to delayed fluorescence. To explain the power-law statistics of the delayed fluorescence (Figure 1b, main manuscript) and of the "on"- and "off"-durations (Figure 3d, main manuscript), we need to assume that the detrapping rate is not fixed, but detrapping rates are distributed over a wide range of time scales. This assumption corresponds, for example, to the multiple trap model where a uniform spatial distribution of trap states is present in a nanocrystal in which the charge carriers can be trapped (*e.g. via* tunneling). When the charge remains trapped for a time exceeding the time of the inverse repetition rate of the laser, a trion state (T) can be excited. The trion state can be also generated from a biexciton state, where one of the charge carriers can get trapped. We assume, that the trapping rate $\Gamma_{XX,trap}$ is higher compared to $\Gamma_{X,trap,}$ since more charge carriers are inside the quantum dot. Probably, the trapping of the XX state is also affected by Coulomb repulsion of charge carriers of the same charge. This trion state can emit a photon radiatively, or the emission can be quenched, presumably by Auger recombination, explaining the "off"-states observed in many measurements. However, in our measurements of single nanocrystals, we observe that the trion state is not completely

dark, but the intensity of the trion state is reduced to ~30 – 40%. Hence, the nonradiative recombination rate is roughly 1.5 times as high as the radiative trion recombination rate ($\Gamma^{Auger}_{T} = 1.5 \cdot \Gamma^{Rad}_{T}$). In our single quantum dot experiment we measure an effective trion decay of 261 ps. Using the efficiency of 40%, we can estimate the radiative trion decay rate $\Gamma^{Rad}_{T} = 650\ ps^{-1}$. In single-nanocrystal measurements, we so far only observed emission from excitons and trions, but we never observed a biexciton emission peak, because although additional peaks may appear with some quantum dots at higher excitation fluence (see Figure S7a of ref. 1), none showed the expected quadratic dependence on the excitation fluence. Therefore, we conclude that either the nonradiative Auger recombination rate is much higher compared to the radiative biexciton recombination rate $\Gamma^{Auger}_{XX} >> \Gamma^{Rad}_{XX}$, or that the trapping rate is dominant ($\Gamma_{XX,trap} >> \Gamma^{Auger}_{XX}, \Gamma^{Rad}_{XX}$). Since other reports measure a non-zero biexciton QY[9], we want to generalize our simulations and assume $\Gamma_{XX,trap}=\Gamma^{Auger}_{XX} =\Gamma^{Rad}_{XX}$ = 1/200 ps. Therefore, the simulations result in a $g^2(0) > 0$ as it can be seen in Figure S6, which is in good agreement with reported values for single $CsPbBr_3$ quantum dots. The effect of choosing different biexciton radiative decay, Auger, and trapping rates on the long decay component and on the blinking statistic is found to be negligible. To explain the delayed fluorescence from the low-intensity trion state, we include in our model that another charge carrier can be trapped when the quantum dot is in the trion state. When one of the two charge carriers is then detrapped, subsequent trion emission leads to delayed fluorescence, which we measure as the long decay component of the low-intensity bins. For simplicity, we assume that both trapped charge carriers are the same, but of course, also other scenarios are possible. In the case when, for example, two electrons are trapped, the probability that a detrapping process occurs is twice as high. This might explain why the absolute value of the exponent of the long decay component of the low-intensity photoluminescence-decay trace is higher, compared to the value of the high-intensity decay trace. We accounted for this with different distributions of detrapping rates.

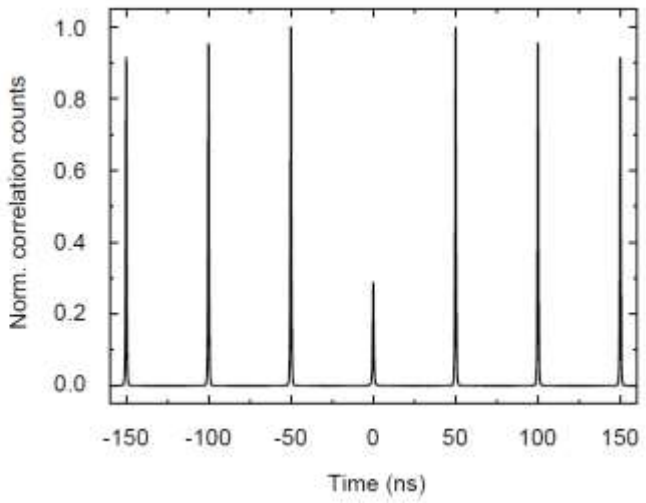

Figure S6. Second-order correlation function with a $g^{(2)}(0) = 0.3$ of the simulated data shown in Figure 5.

S7. Monte Carlo Simulations

Using the above described model, we can quantitatively reproduce the fluorescence dynamics that we observe in the experiment. The model uses the standard kinetic Monte Carlo method[10] to describe the microscopic processes in a single quantum dot. For each state (X, XX, T, ...) in the model, shown in Figure 5, M possible transitions to other states exist, as indicated by the gray arrows with different rates Γ_i. Hence, the probability that the quantum dot will undergo a transition to a state j is given by $\rho_j = \frac{\Gamma_j}{\sum_{i=0..M} \Gamma_i}$. Hereupon, we subdivide the range [0, 1] into M parts, each with the length equal to a probability ρ_i with $i = 0..M$. The transition is then selected by a uniform random number between zero and unity. To calculate the residence time of the current state, we use $\Delta t = -\ln U / \sum_i \Gamma_i$, where U is again a random number between zero and unity ($U \epsilon [0,1]$). For every radiative decay that occurs in our model, we note the absolute time T and the time after the last excitation t. To realistically model pulsed excitation, we directly excite the quantum dot to the exciton or biexciton state, as soon as the quantum dot

reaches the ground state and add the remaining time until the next pulse to the absolute time *T*. Furthermore, when the trapping time exceeds the repetition time of the laser ($\tau_{Laser} = 1/\Gamma_{Rep}$) and the quantum dot is either in the exciton (X) or the trapped exciton (Trapped X) state, the quantum dot is promoted to the biexciton (XX) or trion (T) state, respectively, with the probability n_X. Every time a detrapping (recovery) process happens, a new detrapping rate is randomly assigned to the particular process. This aims to simulate, for example, many traps in a single quantum dot, explaining the power-law statistics of the long decay component. For all detrapping processes, we chose a range of rates between $1 \cdot 10^{-3} - 1 \cdot 10^{-12}$ ps^{-1} and a power-law distribution of the rates over the whole range. To observe blinking events on the second-time scale with long "on"-states and delayed fluorescence on the nanosecond time scale, we need to assume that the occurrence of high detrapping rates is much higher compared to the occurrence of low detrapping rates. If this is not the case, the quantum dot would be mainly in the "off"-state. Nevertheless, the actual distribution of detrapping rates remains unknown, and for simplicity, we choose a power-law dependence with a higher occurrence for fast detrapping rates compared to slow rates. For the detrapping rate from the state where both electrons are trapped (see Figure 5a) to the trion state, we chose a steeper distribution compared to the single trapped charge case, since the probability that one of the two electrons recover should be higher. Figure 5b shows the simulated emission intensity trace over 10 s with a bin size of 10 ms in the absence of shot noise, showing fast switching between two intensity levels, as observed in the experiment. Furthermore, with this Monte Carlo simulation we can also quantitatively reproduce the photoluminescence decays of the exciton and trion state in Figure 5c in gray and red, respectively, both showing a short exponential and long power-law decay with distinct rates. To better compare the simulation with the results obtained from the time-tagged time-resolved measurement, we followed the same procedure and plot the photoluminescence decays for two different intensity levels [0 – 0.5] and [0.6 – 1.0] of the simulated emission intensity

trace with a bin size of 10 ms in Figure 5d. By comparing Figure 5c and Figure 5d, we observe that the decays have a high similarity and that the long decay components of the exciton in Figure 5c and the high-intensity bins in Figure 5d have both a power-law exponent. We note that with the used probability distribution of detrapping rates the power-law exponents of the photoluminescence decays cannot accurately be matched with the experiment. To obtain an even better match between the model result and experiment, it is possible to adjust the probability distributions of the detrapping rates with the constraint that the occurrence of the high detrapping rates must be much higher compared to the occurrence of low detrapping rates. Different distributions of detrapping rates show similar results[7] and fit both the blinking statistics and the power-law exponents. However, for simplicity we want to restrict to the discussed case and show that the main characteristic features of blinking and delayed fluorescence in both the exciton and trion state can be explained with the above described model.

S8. Blinking with Three Intensity Levels

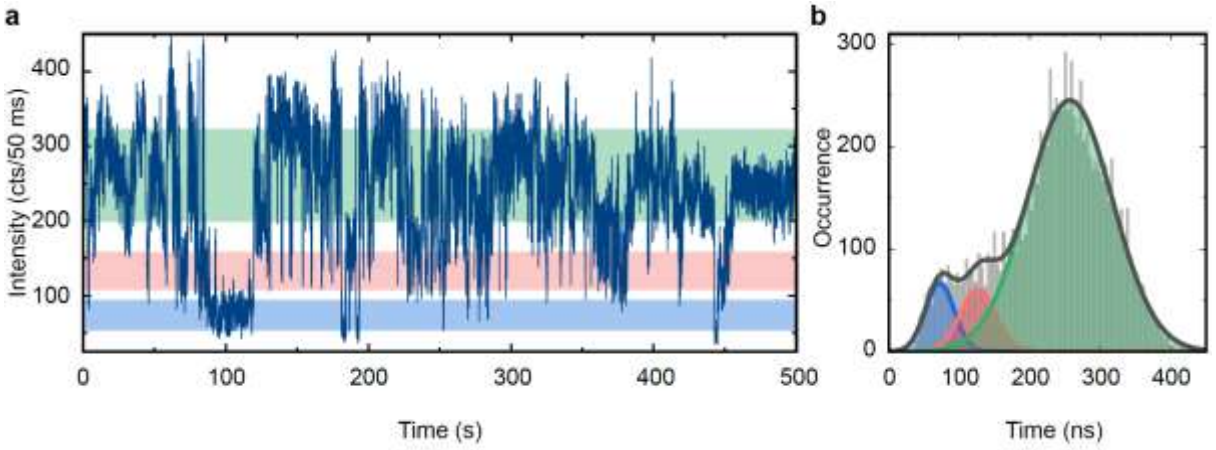

Figure S7. Intensity–time trace with blinking events between three intensity levels. (a) Intensity–time trace of a single $CsPbBr_3$ quantum dot with a bin size of 50 ms. Random

switching events between three intensity levels can be seen that can be naturally explained by the above described microscopic blinking model. (b) Histogram of the corresponding intensity trace in (a) with a fit of three Gaussian functions to the data represented by the solid lines. The shaded areas in (a) are a guide to the eye, representing the intensity-count maximum of the Gaussian fits and their respective full-width at half-maximum.

Noteworthy to mention, this model naturally explains the occurrence of a third intensity level, which is often referred to as gray state[11,12] observed occasionally in single perovskite quantum dots, as exemplary shown in Figure S7 for a single $CsPbBr_3$ nanocrystal with a size of 6 nm. A third intensity level can be observed in the intensity–time trace if a second charge carrier is trapped and the detrapping time exceeds the bin size of the time trace. Again, this is strongly dependent on the probability distributions of the detrapping rates.

REFERENCES

(1) Rainò, G.; Nedelcu, G.; Protesescu, L.; Bodnarchuk, M. I.; Kovalenko, M. V.; Mahrt, R. F.; Stöferle, T. Single Cesium Lead Halide Perovskite Nanocrystals at Low Temperature: Fast Single Photon Emission, Reduced Blinking, and Exciton Fine Structure. *ACS Nano* **2016**, *10*, 2485.

(2) Fu, M.; Tamarat, P.; Huang, H.; Even, J.; Rogach, A. L.; Lounis, B. Neutral and Charged Exciton Fine Structure in Single Lead Halide Perovskite Nanocrystals Revealed by Magneto-Optical Spectroscopy. *Nano Lett.* **2017**, *17*, 2895.

(3) Lv, Y.; Yin, C.; Zhang, C.; Yu, W. W.; Wang, X.; Zhang, Y.; Xiao, M. Quantum Interference in a Single Perovskite Nanocrystal. *Nano Lett.* **2019**, *19*, 4442.

(4) Galland, C.; Ghosh, Y.; Steinbrück, A.; Sykora, M.; Hollingsworth, J. A.; Klimov, V. I.; Htoon, H. Two Types of Luminescence Blinking Revealed by Spectroelectrochemistry of Single Quantum Dots. *Nature* **2011**, *479*, 203.

(5) Moerner, W. Those Blinking Single Molecules. *Science* **1997**, *277*, 1059.

(6) Efros, A. L.; Rosen, M. Random Telegraph Signal in the Photoluminescence Intensity of a Single Quantum Dot. *Phys. Rev. Lett.* **1997**, *78*, 1110.

(7) Ye, M.; Searson, P. C. Blinking in Quantum Dots: The Origin of the Grey State and Power Law Statistics. *Phys. Rev. B* **2011**, *84*, 125317.

(8) Efros, A. L.; Nesbitt, D. J. Origin and Control of Blinking in Quantum Dots. *Nat. Nanotechnol.* **2016**, *11*, 661.

(9) Utzat, H.; Shulenberger, K. E.; Achorn, O. B.; Nasilowski, M.; Sinclair, T. S.; Bawendi, M. G. Probing Linewidths and Biexciton Quantum Yields of Single Cesium Lead Halide Nanocrystals in Solution. *Nano Lett.* **2017**, *17*, 6838.

(10) Fichthorn, K. A.; Weinberg, W. H. Theoretical Foundations of Dynamical Monte Carlo Simulations. *J. Chem. Phys.* **1991**, *95*, 1090.

(11) Spinicelli, P.; Buil, S.; Quelin, X.; Mahler, B.; Dubertret, B.; Hermier, J.-P. Bright and Grey States in CdSe-CdS Nanocrystals Exhibiting Strongly Reduced Blinking. *Phys. Rev. Lett.* **2009**, *102*, 136801.

(12) Tenne, R.; Teitelboim, A.; Rukenstein, P.; Dyshel, M.; Mokari, T.; Oron, D. Studying Quantum Dot Blinking through the Addition of an Engineered Inorganic Hole Trap. *ACS Nano* **2013**, *7*, 5084.